An integral equation solution to the geophysical electromagnetic forward-modelling problem

Colin G. Farquharson and Douglas W. Oldenburg,

UBC – Geophysical Inversion Facility, Department of Earth & Ocean Sciences, University of British Columbia, Vancouver, Canada.

Abstract

We investigate the use of edge element basis vectors in an integral equation solution for three-dimensional geophysical electromagnetic modelling. Expansion of the total electric field within the region of anomalous conductivity in terms of these basis vectors gives a bilinear variation of each component of the field within a cell in the two directions perpendicular to the component (and so a divergence free but not curl free field within a cell), and continuity of the tangential electric field between two cells. In addition, we use a form of the electric field integral equation that explicitly involves the charge densities on cell faces associated with any discontinuity of the normal component of the current density. The two types of integrals in the integral equation – the volume integration of the scattering current within each cell, and the surface integration of the charge density on the faces of each cell – are computed using Gaussian quadrature. The system of equations to be solved is constructed using the Galerkin approach. In this preliminary study, we consider the simple case of a homogeneous halfspace as the background model. Comparisons with results from the literature and other codes have been promising. We include here two examples: one for a grounded electric line source at low frequency ($3\,\mathrm{Hz}$) on the surface of a halfspace ($\sigma = 0.02\,\mathrm{S/m}$) in which a more conductive vertical prism ($\sigma = 0.2\,\mathrm{S/m}$) is buried, and one for a magnetic dipole source-receiver combination over a conductive cube ($\sigma = 100\,\mathrm{S/m}$) in a resistive ($\sigma = 10^{-4}\,\mathrm{S/m}$) background.

Keywords: Electromagnetics, three-dimensional, forward modelling, integral equation, edge elements, high contrast.

1. Introduction

Traditional integral equation formulations for electromagnetic modelling in geophysics (e.g., Hohmann, 1975), which use pulse basis functions to represent the electric field, fail for

1

large conductivity contrasts. Newman & Hohmann (1988) provide a means of remedying this problem by grouping together pulse basis functions to explicitly form current loops. We have implemented, as we shall describe, the more sophisticated edge element basis functions in the anticipation that the inaccuracies of the traditional approach can be avoided. Edge element basis functions have desirable properties: they are divergence free but not curl free, and give a solution for which the tangential electric field is, by construction, continuous across cell faces. They have been successfully used in finite element solutions to electromagnetic forward modelling (e.g., Jin, 1993). The use of similarly sophisticated, although different, basis functions (linear variation of each electric field component in all three dimensions, and imposition of continuity of tangential field components and normal current density) has been presented by Slob & van den Berg (1999).

We start by deriving the form of the integral equation upon which our numerical solution is based, a form that explicitly involves the charge densities on cell faces across which there is a difference in conductivity, and thus directly reduces at zero frequency to the integral equation solution for the direct-current (DC) resistivity forward-modelling problem.

2. The integral equation

Consider Maxwell's two curl equations in the frequency domain (assuming a time dependence of $e^{-i\omega t}$, and the quasi-static approximation):

$$\nabla \times \mathbf{E} \ = \ i\omega\mu\mathbf{H}, \tag{1}$$

$$\nabla \times \mathbf{H} \ = \ \sigma\mathbf{E} \ + \ \mathbf{J}^I, \tag{2}$$

and the statement of conservation of charge:

$$\nabla \cdot \left(\sigma\mathbf{E}\right) \ = \ -\nabla \cdot \mathbf{J}^I, \tag{3}$$

where $\mathbf{E}(\mathbf{r},\omega)$ and $\mathbf{H}(\mathbf{r},\omega)$ are the total electric and magnetic fields, $\mu = \mu_0$ is the magnetic permeability of free space, $\sigma = \sigma(\mathbf{r})$ is the electrical conductivity of our model Earth, and $\mathbf{J}^I$ is the impressed electric current density. Taking the curl of eq. (1), using eq. (2) to eliminate $\mathbf{H}$, and exploiting the vector identity $\nabla \times \nabla \times \mathbf{E} = -\nabla^2\mathbf{E} + \nabla\left(\nabla \cdot \mathbf{E}\right)$, gives

$$-\nabla^2\mathbf{E} \ + \ \nabla\left(\nabla \cdot \mathbf{E}\right) \ - \ i\omega\mu\sigma\mathbf{E} \ = \ i\omega\mu\mathbf{J}^I. \tag{4}$$

Consider now a background conductivity $\sigma_b(\mathbf{r})$, and the electric and magnetic fields $\mathbf{E}_b$ and $\mathbf{H}_b$ that exist in this background model for the impressed current density $\mathbf{J}^I$. The two Maxwell's curl equations for this scenario are

$$\nabla \times \mathbf{E}_b \;=\; i\omega\mu\mathbf{H}_b, \tag{5}$$

$$\nabla \times \mathbf{H}_b \;=\; \sigma_b\mathbf{E}_b \;+\; \mathbf{J}^I, \tag{6}$$

and the statement of conservation of charge is

$$\nabla \cdot \left(\sigma_b\mathbf{E}_b\right) \;=\; -\nabla \cdot \mathbf{J}^I. \tag{7}$$

Performing the same manipulations as for the total fields gives

$$-\nabla^2\mathbf{E}_b \;+\; \nabla\left(\nabla \cdot \mathbf{E}_b\right) \;-\; i\omega\mu\sigma_b\mathbf{E}_b \;=\; i\omega\mu\mathbf{J}^I. \tag{8}$$

Now consider the total electric field in the model with $\sigma = \sigma(\mathbf{r})$ to be the sum of the background electric field and a "secondary" part: $\mathbf{E} = \mathbf{E}_b + \mathbf{E}_s$. Also consider $\sigma(\mathbf{r}) = \sigma_b(\mathbf{r}) + \Delta\sigma(\mathbf{r})$. Substituting these two expressions into eq. (4) gives

$$-\nabla^2\left(\mathbf{E}_b \;+\; \mathbf{E}_s\right) \;+\; \nabla\left(\nabla \cdot \left(\mathbf{E}_b + \mathbf{E}_s\right)\right) \;-\; i\omega\mu\left(\sigma_b + \Delta\sigma\right)\left(\mathbf{E}_b + \mathbf{E}_s\right) \;=\; i\omega\mu\mathbf{J}^I. \tag{9}$$

Expanding the terms in parentheses, and using eq. (8) to cancel many of the resulting terms, gives

$$-\nabla^2\mathbf{E}_s \;+\; \nabla\left(\nabla \cdot \mathbf{E}_s\right) \;-\; i\omega\mu\sigma_b\mathbf{E}_s \;=\; i\omega\mu\Delta\sigma\mathbf{E}. \tag{10}$$

Likewise substituting $\mathbf{E} = \mathbf{E}_b + \mathbf{E}_s$ and $\sigma = \sigma_b + \Delta\sigma$ into eq. (3), and using eq. (7) to eliminate $\mathbf{J}^I$, gives

$$\nabla \cdot \mathbf{E}_s \;=\; -\frac{1}{\sigma_b}\nabla\sigma_b \cdot \mathbf{E}_s \;-\; \frac{1}{\sigma_b}\nabla \cdot \left(\Delta\sigma\,\mathbf{E}\right). \tag{11}$$

We now assume that our background model is a homogeneous halfspace, meaning that $\nabla\sigma_b$ is non-zero only on the Earth-air interface (at $z = 0$). Rewriting eq. (11) using more symbolic terms that avoid derivatives of conductivity discontinuities (both at the Earth-air interface and between cells once we discretize the anomalous region) gives

$$\nabla \cdot \mathbf{E}_s \;=\; \nabla \cdot \mathbf{E}_s\big|_{z=0} \;+\; \nabla \cdot \mathbf{E}_s\big|_{V_a}, \tag{12}$$

where the first term on the right-hand side represents the contribution from the Earth-air interface, and the second term represents the contribution from the region of anomalous

conductivity (which occupies the volume V_a). The differential equation for the secondary electric field (eq. 10) therefore becomes (cf. Hohmann, 1987)

$$\nabla^2\mathbf{E}_s \; - \; \nabla\big(\nabla\cdot\mathbf{E}_s|_{z=0}\big) \; + \; i\omega\mu\sigma_b\mathbf{E}_s \; = \; -i\omega\mu\Delta\sigma\mathbf{E} \; + \; \nabla\big(\nabla\cdot\mathbf{E}_s|_{V_a}\big). \tag{13}$$

Rewriting this equation using notation that simplifies the right-hand side:

$$\nabla^2\mathbf{E}_s \; - \; \nabla\big(\nabla\cdot\mathbf{E}_s|_{z=0}\big) \; + \; i\omega\mu\sigma_b\mathbf{E}_s \; = \; \mathbf{Q}, \tag{14}$$

where $\mathbf{Q} = -i\omega\mu\Delta\sigma\mathbf{E} + \nabla(\nabla\cdot\mathbf{E}_s|_{V_a})$. Consider now a vector Green's function $\mathbf{g}^k$ such that

$$\nabla^2\mathbf{g}^k(\mathbf{r};\mathbf{r}') \; - \; \nabla\big(\nabla\cdot\mathbf{g}^k(\mathbf{r};\mathbf{r}')|_{z=0}\big) \; + \; i\omega\mu\sigma_b\mathbf{g}^k(\mathbf{r};\mathbf{r}') \; = \; -\delta(\mathbf{r}-\mathbf{r}')\,\hat{\mathbf{u}}_k, \tag{15}$$

where $\hat{\mathbf{u}}_k$ is the unit vector in the kth direction. All components of $\mathbf{g}^k \to 0$ as $|\mathbf{r}| \to \infty$. What conditions $\mathbf{g}^k$ satisfies on the Earth-air interface will be discussed in Section 7. Taking the scalar product of $\mathbf{g}^k(\mathbf{r};\mathbf{r}')$ and eq. (14), the scalar product of $\mathbf{E}_s$ and eq. (15), subtracting the second resulting equation from the first, and integrating over all space, gives

$$\int_V \Big\{\mathbf{g}^k\cdot\big[\nabla^{2'}\mathbf{E}_s \; - \; \nabla'(\nabla'\cdot\mathbf{E}_s|_0) + i\omega\mu\sigma_b\mathbf{E}_s\big] \; -$$

$$\mathbf{E}_s\cdot\big[\nabla^{2'}\mathbf{g}^k \; - \; \nabla'(\nabla'\cdot\mathbf{g}^k|_0) \; + \; i\omega\mu\sigma_b\mathbf{g}^k\big]\Big\}\,dv'$$

$$= \; \int_V \Big\{\mathbf{g}^k\cdot\mathbf{Q} \; + \; \mathbf{E}_s\cdot\delta(\mathbf{r}-\mathbf{r}')\hat{\mathbf{u}}_k\Big\}\,dv'. \tag{16}$$

Simplifying both the right- and left-hand sides gives

$$\int_V \big\{\mathbf{g}^k\cdot\nabla^{2'}\mathbf{E}_s \; - \; \mathbf{E}_s\cdot\nabla^{2'}\mathbf{g}^k\big\}\,dv' \; - \; \int_V \big\{\mathbf{g}^k\cdot\nabla'(\nabla'\cdot\mathbf{E}_s|_0) \; - \; \mathbf{E}_s\cdot\nabla'(\nabla'\cdot\mathbf{g}^k|_0)\big\}\,dv'$$

$$= \; \int_V \mathbf{g}^k\cdot\mathbf{Q}\,dv' \; + \; E_k^s, \tag{17}$$

where E_k^s is the kth component of the secondary electric field. Rewriting the first integral on the left-hand side of the above equation in terms of the components of $\mathbf{E}_s$ and $\mathbf{g}^k$ gives

$$\int_V \big\{\mathbf{g}^k\cdot\nabla^{2'}\mathbf{E}_s \; - \; \mathbf{E}_s\cdot\nabla^{2'}\mathbf{g}^k\big\}\,dv' \; = \; \int_V \big\{g_x^k\nabla^{2'}E_x^s - E_x^s\nabla^{2'}g_x^k\big\}\,dv' \; +$$

$$\int_V \big\{g_y^k\nabla^{2'}E_y^s - E_y^s\nabla^{2'}g_y^k\big\}\,dv' \; + \; \int_V \big\{g_z^k\nabla^{2'}E_z^s - E_z^s\nabla^{2'}g_z^k\big\}\,dv', \tag{18}$$

$$= \; \int_{\partial V} \big\{g_x^k\nabla'E_x^s - E_x^s\nabla'g_x^k\big\}\cdot\hat{\mathbf{n}}\,ds' \; +$$

$$\int_{\partial V} \big\{g_y^k\nabla'E_y^s - E_y^s\nabla'g_y^k\big\}\cdot\hat{\mathbf{n}}\,ds' \; + \; \int_{\partial V} \big\{g_z^k\nabla'E_z^s - E_z^s\nabla'g_z^k\big\}\cdot\hat{\mathbf{n}}\,ds', \tag{19}$$

using the second scalar Green's theorem (Tai, 1993). But these three surface integrals vanish because all components of $\mathbf{E}_s$ and $\mathbf{g}^k$ are zero on the boundary ∂V (at infinity). Integrating by parts the second integral of the left-hand side of eq. (17) gives

$$
\int_V \left\{ \mathbf{g}^k \cdot \nabla'(\nabla' \cdot \mathbf{E}_s|_0) - \mathbf{E}_s \cdot \nabla'(\nabla' \cdot \mathbf{g}^k|_0) \right\} dv'
$$

$$
= \int_V \left\{ \nabla' \cdot \mathbf{g}^k \, \nabla' \cdot \mathbf{E}_s|_0 - \nabla' \cdot \mathbf{E}_s \, \nabla' \cdot \mathbf{g}^k|_0 \right\} dv', \tag{20}
$$

$$
= \int_{-\infty}^{\infty} \int_{-\infty}^{\infty} \left\{ \nabla' \cdot \mathbf{g}^k|_{z=0} \, \nabla' \cdot \mathbf{E}_s|_{z=0} - \nabla' \cdot \mathbf{E}_s|_{z=0} \, \nabla' \cdot \mathbf{g}^k|_{z=0} \right\} dx' \, dy', \tag{21}
$$

which is equal to zero. Hence, from eq. (17), and reinstating $\mathbf{Q}$,

$$
E_k^s = i\omega\mu \int_V \mathbf{g}^k \cdot \mathbf{E} \, \Delta\sigma \, dv' - \int_V \mathbf{g}^k \cdot \nabla'(\nabla' \cdot \mathbf{E}_s|_{V_a}) \, dv'. \tag{22}
$$

Integrating the second term on the right-hand side by parts, and using the fact that $\mathbf{g}^k$ is zero on the boundary, gives

$$
E_k^s = i\omega\mu \int_V \mathbf{g}^k \cdot \mathbf{E} \, \Delta\sigma \, dv' + \int_V \nabla' \cdot \mathbf{g}^k \, \nabla' \cdot \mathbf{E}_s|_{V_a} \, dv'. \tag{23}
$$

Considering the three components of the secondary electric field, and adding the background electric field to both sides, gives the vector integral equation:

$$
\mathbf{E} = \mathbf{E}_b + i\omega\mu \int_V \underline{\mathbf{G}}^{(1)} \cdot \mathbf{E} \, \Delta\sigma \, dv' + \int_V \mathbf{G}^{(2)} \, \nabla' \cdot \mathbf{E}_s|_{V_a} \, dv', \tag{24}
$$

where

$$
\underline{\mathbf{G}}^{(1)} = \begin{pmatrix} g_x^x & g_y^x & g_z^x \\ g_x^y & g_y^y & g_z^y \\ g_x^z & g_y^z & g_z^z \end{pmatrix} \quad \text{and} \quad \mathbf{G}^{(2)} = \begin{pmatrix} \nabla' \cdot \mathbf{g}^x \\ \nabla' \cdot \mathbf{g}^y \\ \nabla' \cdot \mathbf{g}^z \end{pmatrix}. \tag{25}
$$

This integral equation as written reduces at zero frequency to the integral equation for the DC resistivity problem, and we ensure this correspondence remains intact between our numerical implementation of eq. (24) and numerical implementations for the DC problem (e.g., Snyder, 1976).

The integral equation for the magnetic field is obtained from eq. (24) by $\mathbf{H} = \nabla \times \mathbf{E}/i\omega\mu$:

$$
\mathbf{H} = \mathbf{H}_b + \int_V \underline{\mathbf{G}}^{(3)} \cdot \mathbf{E} \, \Delta\sigma \, dv', \tag{26}
$$

where each column of $\underline{\mathbf{G}}^{(3)}$ is given by $1/(i\omega\mu)\,\nabla\times$ of each column of $\underline{\mathbf{G}}^{(1)}$. The second integral in eq. (24) does not contribute to the magnetic field.

3. Numerical solution – Galerkin approach

The numerical solution of the integral equation is obtained using the method of weighted residuals. The only contributions to both integrals in eq. (24) are from the anomalous region. Since our background model is a homogeneous halfspace, $\nabla\cdot\mathbf{E}_b$ is zero within this region, and we can therefore replace $\nabla\cdot\mathbf{E}_s$ in eq. (24) by $\nabla\cdot\mathbf{E}$, giving, after re-ordering the terms and explicitly limiting the integrations to the anomalous region V_a,

$$\mathbf{E} \;-\; i\omega\mu\int_{V_a}\underline{\mathbf{G}}^{(1)}\cdot\mathbf{E}\,\Delta\sigma\,dv' \;-\; \int_{V_a}\mathbf{G}^{(2)}\,\nabla'\cdot\mathbf{E}\,dv' \;=\; \mathbf{E}_b, \tag{27}$$

which is a linear operator acting on the total electric field:

$$\mathbf{L}\big[\mathbf{E}\big] \;=\; \mathbf{E}_b. \tag{28}$$

The total electric field is expressed as a linear combination of basis vectors:

$$\mathbf{E}(\mathbf{r}) \;\approx\; \sum_{j=1}^{N}c_j\,\mathbf{v}_j(\mathbf{r}). \tag{29}$$

Substituting this representation into eq. (28) gives

$$\sum_{j=1}^{N}c_j\,\mathbf{L}\big[\mathbf{v}_j\big] \;=\; \mathbf{E}_b \;+\; \mathbf{R}, \tag{30}$$

where the residual $\mathbf{R}$ represents the error introduced by the approximation in eq. (29). Taking the inner product of eq. (30) with each of a set of weight functions, $\mathbf{w}_i(\mathbf{r}), i = 1,\ldots,M$, and requiring that the residual $\mathbf{R}$ be orthogonal to these weight functions, that is, $\langle\mathbf{w}_i,\mathbf{R}\rangle = 0$ for all i, results in the matrix equation

$$\underline{\mathbf{A}}\,\mathbf{x} \;=\; \mathbf{b}, \tag{31}$$

where $A_{ij} = \langle\mathbf{w}_i,\mathbf{L}[\mathbf{v}_j]\rangle$, $x_i = c_i$, and $b_i = \langle\mathbf{w}_i,\mathbf{E}_b\rangle$. The inner product is defined as $\langle\mathbf{w},\mathbf{v}\rangle = \int_V\mathbf{w}\cdot\mathbf{v}\,dv'$. We adopt the Galerkin approach in which the basis vectors are used as the weight functions.

4. Edge element basis vectors

It is assumed that the region of anomalous conductivity can be represented by a grid of cuboidal cells within each of which the conductivity is uniform. Within a cell, we approximate the total electric field by a linear combination of twelve basis vectors, four directed in the x-direction, four directed in the y-direction, and four in the z-direction. The four basis vectors directed in the x-direction vary bilinearly with y & z, the four in the y-direction vary with x & z, and those in the z-direction vary with x & y. The total electric field within each cell is therefore divergence free by construction. It can also have a non-zero curl.

Explicitly, the x-component of the electric field in an example cell (see Figure 1a) is given by (e.g., Jin, 1993):

$$E_x(\mathbf{r})\,\hat{\mathbf{u}}_x = c_1\,\mathbf{v}_1(\mathbf{r}) \;+\; c_2\,\mathbf{v}_2(\mathbf{r}) \;+\; c_3\,\mathbf{v}_3(\mathbf{r}) \;+\; c_4\,\mathbf{v}_4(\mathbf{r}), \tag{32}$$

$$\begin{aligned}
&= c_1\left\{(y - y_c + l_y)(z - z_c + l_z)/4l_y l_z\right\}\hat{\mathbf{u}}_x + \\
&\quad c_2\left\{(y_c + l_y - y)(z - z_c + l_z)/4l_y l_z\right\}\hat{\mathbf{u}}_x + \\
&\quad c_3\left\{(y - y_c + l_y)(z_c + l_z - z)/4l_y l_z\right\}\hat{\mathbf{u}}_x + \\
&\quad c_4\left\{(y_c + l_y - y)(z_c + l_z - z)/4l_y l_z\right\}\hat{\mathbf{u}}_x,
\end{aligned} \tag{33}$$

where y_c and z_c are the y- and z-coordinates of the centre of the cell, and $2\,l_y$ and $2\,l_z$ are the extents of the cell in the y- and z-directions. With the above definitions of these four basis vectors, $v_1 = 1$ & $v_2 = v_3 = v_4 = 0$ on the edge of the cell with $y = y_c + l_y$ & $z = z_c + l_z$, $v_2 = 1$ & $v_1 = v_3 = v_4 = 0$ on the edge with $y = y_c - l_y$ & $z = z_c + l_z$, and likewise for the other two edges. The x-component of the electric field is thus effectively equal to c_1, c_2, c_3 & c_4 respectively on the x-directed edges of the cell (see Figure 1a).

In an analogous manner to eq. (33), the y-component of the electric field within this example cell is given by

$$\begin{aligned}
E_y(\mathbf{r})\,\hat{\mathbf{u}}_y &= c_5\left\{(x - x_c + l_x)(z - z_c + l_z)/4l_x l_z\right\}\hat{\mathbf{u}}_y + \\
&\quad c_6\left\{(x_c + l_x - x)(z - z_c + l_z)/4l_x l_z\right\}\hat{\mathbf{u}}_y + \\
&\quad c_7\left\{(x - x_c + l_x)(z_c + l_z - z)/4l_x l_z\right\}\hat{\mathbf{u}}_y + \\
&\quad c_8\left\{(x_c + l_x - x)(z_c + l_z - z)/4l_x l_z\right\}\hat{\mathbf{u}}_y,
\end{aligned} \tag{34}$$

and the z-component of the electric field by

$$
\begin{aligned}
E_z(\mathbf{r})\,\hat{\mathbf{u}}_z \;=\; & c_9 \left\{ (x - x_c + l_x)(y - y_c + l_y)/4l_x l_y \right\} \hat{\mathbf{u}}_z \;+ \\
& c_{10} \left\{ (x_c + l_x - x)(y - y_c + l_y)/4l_x l_y \right\} \hat{\mathbf{u}}_z \;+ \\
& c_{11} \left\{ (x - x_c + l_x)(y_c + l_y - y)/4l_x l_y \right\} \hat{\mathbf{u}}_z \;+ \\
& c_{12} \left\{ (x_c + l_x - x)(y_c + l_y - y)/4l_x l_y \right\} \hat{\mathbf{u}}_z,
\end{aligned}
\tag{35}
$$

where x_c is the x-coordinate of the centre of the cell and $2\,l_x$ is the extent of the cell in the x-direction.

When two cells share a face, the basis function in the one cell that is equal to 1 on one of the shared edges and the basis function in the other cell that is equal to 1 on the same edge are treated as a single basis vector, meaning their coefficients are then equal. Consider, for example, the two cells in Figure 1(b) which share the face for which $y = y_c^{(1)} + l_y^{(1)} = y_c^{(2)} - l_y^{(2)}$, where the superscripts indicate the number of the cell. Suppose the basis vectors for $j = 1, \ldots, 12$ apply to cell 1 and those for $j = 13, \ldots, 24$ apply to cell 2. This means that both v_1 and v_{14} are equal to 1 on the edge for which $y = y_c^{(1)} + l_y^{(1)} = y_c^{(2)} - l_y^{(2)}$ & $z = z_c^{(1)} + l_z^{(1)} = z_c^{(2)} + l_z^{(2)}$, and both v_3 and v_{16} are equal to 1 on the edge for which $y = y_c^{(1)} + l_y^{(1)} = y_c^{(2)} - l_y^{(2)}$ & $z = z_c^{(1)} - l_z^{(1)} = z_c^{(2)} - l_z^{(2)}$. These four basis vectors are therefore considered as just two distinct basis vectors: $(v_1 + v_{14})$ & $(v_3 + v_{16})$ with coefficients $\tilde{c}_1 = c_1 = c_{14}$ & $\tilde{c}_3 = c_3 = c_{16}$. This tying together of basis vectors associated with shared cell edges is implemented by summing the corresponding columns and rows of the system of equations in eq. (31). The consequence is that the tangential component of the total electric field is continuous, by construction, across any interface between cells.

5. The Green's functions – part I

Our background model is a homogeneous halfspace. However, to simplify the computations required when constructing eq. (31), it is assumed that the anomalous region is sufficiently far from the Earth-air interface that, when both $\mathbf{r}$ & $\mathbf{r}'$ are within the anomalous region, the contributions to the Green's functions $\underline{\mathbf{G}}^{(1)}$ & $\mathbf{G}^{(2)}$ from the Earth-air interface can be ignored. Hence, $\underline{\mathbf{G}}^{(1)}$ is a diagonal tensor whose elements are all equal to the wholespace Green's function:

$$
g_x^x \;=\; g_y^y \;=\; g_z^z \;=\; g^w(\mathbf{r}; \mathbf{r}') \;=\; \frac{1}{4\pi} \frac{e^{ik_b|\mathbf{r} - \mathbf{r}'|}}{|\mathbf{r} - \mathbf{r}'|},
\tag{36}
$$

8

where $k_b^2 = i\omega\mu\sigma_b$, and

$$\mathbf{G}^{(2)} = \begin{pmatrix} \partial g^w/\partial x' \\ \partial g^w/\partial y' \\ \partial g^w/\partial z' \end{pmatrix} = \nabla' g^w. \tag{37}$$

6. Evaluation of the integrals

The volume integrals associated with the inner products $\langle \mathbf{w}_i, \mathbf{L}[\mathbf{v}_j]\rangle$ and $\langle \mathbf{w}_i, \mathbf{E}_b\rangle$ in eq. (31) are computed using Gaussian quadrature. The two types of integrals associated with $\underline{\mathbf{L}}[\mathbf{v}_j]$ are computed as follows. The first integral, that is,

$$\mathbf{L}^{(1)}[\mathbf{v}_j] = i\omega\mu \int_{V_a} \underline{\mathbf{G}}^{(1)}(\mathbf{r};\mathbf{r}') \cdot \mathbf{v}_j(\mathbf{r}') \Delta\sigma(\mathbf{r}') \, dv', \tag{38}$$

is evaluated using Gaussian quadrature when $\mathbf{r}$ is outside the cell over which the integration is taking place, and using the trapezoidal rule (with typically $10 \times 10 \times 10$ evaluation points) when $\mathbf{r}$ is within the cell so that $\mathbf{r}'$ does not correspond to a Gaussian quadrature node for the inner product integrations. The elements of $\underline{\mathbf{G}}^{(1)}$ are singular at $\mathbf{r}' = \mathbf{r}$ because of their $1/|\mathbf{r} - \mathbf{r}'|$ dependence. However, the singularity does not contribute to the integral. To see this, split the integral in eq. (38) into one part for a sphere of radius ϵ centred on $\mathbf{r}' = \mathbf{r}$, and one part over the rest of the cell in which $\mathbf{v}_j$ is non-zero. For small ϵ, the basis vector can be considered as being constant within the sphere, and the exponential term in the components of $\underline{\mathbf{G}}^{(1)}$ can be considered to be constant and equal to its value for $|\mathbf{r} - \mathbf{r}'| = 0$, which is 1. The integration over the sphere becomes:

$$i\omega\mu \int_{V_\epsilon} \underline{\mathbf{G}}^{(1)}(\mathbf{r};\mathbf{r}') \cdot \mathbf{v}_j(\mathbf{r}') \Delta\sigma(\mathbf{r}') \, dv' \approx i\omega\mu \, \Delta\sigma_J \frac{1}{4\pi} \underline{\mathbf{I}} \cdot \mathbf{v}_j(\mathbf{r}) \int_{\zeta=0}^{\epsilon} \frac{1}{\zeta} 4\pi \zeta^2 \, d\zeta, \tag{39}$$

where $\Delta\sigma_J$ is the anomalous conductivity in the cell, $\underline{\mathbf{I}}$ is the identity tensor, and $\zeta = |\mathbf{r} - \mathbf{r}'|$. This integral vanishes as $\epsilon \to 0$.

The second integral in $\mathbf{L}[\mathbf{v}_j]$ is

$$\mathbf{L}^{(2)}[\mathbf{v}_j] = \int_{V_J} \mathbf{G}^{(2)}(\mathbf{r};\mathbf{r}') \nabla \cdot \mathbf{v}_j(\mathbf{r}') \, dv'. \tag{40}$$

where V_J is the volume of the cell in which $\mathbf{v}_j$ is non-zero. $\nabla \cdot \mathbf{E}$ is non-zero only on the interfaces between cells, where it is equal to the surface charge density (scaled by the permittivity of free space ε_0). Hence (e.g., Li & Oldenburg, 1991),

$$\nabla \cdot \mathbf{v}_j = \left(\frac{\sigma_J}{\sigma_n} - 1\right) \mathbf{v}_j \cdot \hat{\mathbf{n}} \tag{41}$$

9

where σ_J is the conductivity in the cell, σ_n is the conductivity of the neighbouring cell (or of the background if there is no neighbour), and $\hat{\mathbf{n}}$ is the normal to the face of the cell. The integral in eq. (40) therefore becomes

$$\mathbf{L}^{(2)}\left[\mathbf{v}_j\right] \;=\; \int_{\partial V_J} \mathbf{G}^{(2)}(\mathbf{r};\mathbf{r}')\Big(\frac{\sigma_j}{\sigma_n}-1\Big)\mathbf{v}_j(\mathbf{r}')\cdot\hat{\mathbf{n}}\,ds'. \tag{42}$$

The above integrand is singular at $\mathbf{r}' = \mathbf{r}$. This singularity gives rise to a contribution of $2\pi\,\tau(\mathbf{r})/\varepsilon_0$, where τ is the surface charge density (Snyder, 1976). Thus,

$$\mathbf{L}^{(2)}\left[\mathbf{v}_j\right] \;=\; \int_{\partial V_J,\mathbf{r}'\neq\mathbf{r}} \mathbf{G}^{(2)}(\mathbf{r};\mathbf{r}')\Big(\frac{\sigma_j}{\sigma_n}-1\Big)\mathbf{v}_j(\mathbf{r}')\cdot\hat{\mathbf{n}}\,ds' \;-\; 2\pi\,\tau(\mathbf{r})/\varepsilon_0. \tag{43}$$

However, because the second term above exists only on the faces of the cell, it does not contribute to the volume integration over the cell in the calculation of the inner product $\langle\mathbf{w}_i,\mathbf{L}[\mathbf{v}_j]\rangle$, and so can be ignored. The surface integral in eq. (43) is evaluated using Gaussian quadrature.

7. The Green's functions – part II

Once the electric field within the anomalous region is known, the field anywhere can be computed using the simple re-arrangement of eq. (27):

$$\mathbf{E} \;=\; \mathbf{E}_b \;+\; i\omega\mu \int_{V_a} \underline{\mathbf{G}}^{(1)}\cdot\mathbf{E}\,\Delta\sigma\,dv' \;+\; \int_{V_a} \mathbf{G}^{(2)}\,\nabla'\cdot\mathbf{E}\,dv'. \tag{44}$$

The form of $\mathbf{g}^k$, and hence that of $\underline{\mathbf{G}}^{(1)}$ and $\mathbf{G}^{(2)}$, for the homogeneous halfspace is now required. The most straightforward way to see what $\mathbf{g}^x$, $\mathbf{g}^y$ & $\mathbf{g}^z$ should be is to recognize that they are equivalent to the Schelkunoff $\mathbf{A}$-potentials described in Ward & Hohmann (1987) for x-, y- & z-directed electric current density dipole sources. As such, $\mathbf{g}^x$ has only x- and z-components, $\mathbf{g}^y$ only y- and z-components, and $\mathbf{g}^z$ only a z-component. Following eqs. (1.198) – (1.201) of Ward & Hohmann, the components of $\mathbf{g}^x$ satisfy

$$\frac{1}{\sigma_b}\left(\frac{\partial g_x^x}{\partial x} + \frac{\partial g_z^x}{\partial z}\right)\bigg|_{z=0+} \;=\; 0, \tag{45}$$

$$g_z^x\big|_{z=0+} \;=\; g_z^x\big|_{z=0-}, \tag{46}$$

$$g_x^x\big|_{z=0+} \;=\; g_x^x\big|_{z=0-}, \tag{47}$$

$$\frac{\partial g_x^x}{\partial z}\bigg|_{z=0+} \;=\; \frac{\partial g_x^x}{\partial z}\bigg|_{z=0-}, \tag{48}$$

on the surface of the halfspace ($z = 0$, z positive down). The components of $\mathbf{g}^y$ satisfy the same set of conditions with x replaced by y. Following eqs. (1.182) & (1.183) of Ward & Hohmann, the component of $\mathbf{g}^z$ satisfies

$$\frac{1}{\sigma_b} \frac{\partial g_z^z}{\partial z}\bigg|_{z=0+} = 0, \tag{49}$$

$$g_z^z\big|_{z=0+} = g_z^z\big|_{z=0-} . \tag{50}$$

Alternatively, to determine what conditions must be satisfied by $\mathbf{g}^k$ on the Earth-air interface, consider in component form the second and third terms on the right-hand side of eq. (44), that is, the secondary electric field (cf. eq. 23):

$$E_k^s = i\omega\mu \int_{V_a} \mathbf{g}^k \cdot \mathbf{E}\, \Delta\sigma\, dv' + \int_{V_a} \nabla' \cdot \mathbf{g}^k\, \nabla' \cdot \mathbf{E}_s\, dv'. \tag{51}$$

We can rewrite the second integral using eq. (11):

$$E_k^s = i\omega\mu \int_{V_a} \mathbf{g}^k \cdot \mathbf{E}\, \Delta\sigma\, dv' - \int_{V_a} \nabla' \cdot \mathbf{g}^k\, \frac{1}{\sigma_b} \nabla' \cdot \left(\Delta\sigma\, \mathbf{E}\right) dv'. \tag{52}$$

Integrating the second integral by parts gives

$$E_k^s = i\omega\mu \int_{V_a} \mathbf{g}^k \cdot \mathbf{E}\, \Delta\sigma\, dv' + \frac{1}{\sigma_b} \int_{V_a} \nabla'(\nabla' \cdot \mathbf{g}^k) \cdot \mathbf{E}\, \Delta\sigma\, dv', \tag{53}$$

$$= \int_{V_a} \left\{ i\omega\mu\, \mathbf{g}^k + \frac{1}{\sigma_b} \nabla'(\nabla' \cdot \mathbf{g}^k) \right\} \cdot \mathbf{E}\, \Delta\sigma\, dv', \tag{54}$$

where the expression in the braces is the more familiar form of the electric field Green's tensor for a uniform background. Across the Earth-air interface, the tangential components of the secondary E- and H-fields are continuous. In order for our computed values of E_x^s to be continuous, each component of $\left\{ i\omega\mu\, \mathbf{g}^x + \nabla'(\nabla' \cdot \mathbf{g}^x)/\sigma_b \right\}$ must be continuous, and for E_y^s to be continuous, each component of $\left\{ i\omega\mu\, \mathbf{g}^y + \nabla'(\nabla' \cdot \mathbf{g}^y)/\sigma_b \right\}$ must be continuous. Similarly, for H_x^s & H_y^s to be continuous, each component of $\left\{ -\partial_z \mathbf{g}^y + \partial_y \mathbf{g}^z \right\}$ and $\left\{ \partial_z \mathbf{g}^x - \partial_x \mathbf{g}^z \right\}$ must be continuous. Finally, E_z^s is zero on the Earth-air interface. To satisfy this, each component of $\left\{ i\omega\mu\, \mathbf{g}^z + \nabla'(\nabla' \cdot \mathbf{g}^z)/\sigma_b \right\}$ must be zero at $z = 0$. These conditions reduce to the same as those listed in eqs. (45) $-$ (50).

With the above interface conditions, and the defining differential equation (eq. 15) and primary solution (eq. 36), the components of $\mathbf{g}^k$ are determined using standard techniques

(see, for example, Ward & Hohmann, 1987):

$$g_x^x(\mathbf{r};\mathbf{r}') \;=\; g^w(\mathbf{r};\mathbf{r}') \;+\; \frac{1}{2\pi}\int_{\lambda=0}^{\infty}\frac{u-\lambda}{2u(u+\lambda)}\,e^{-u(z+z')}\lambda\,J_0(\lambda\rho)\,d\lambda, \quad z\geq 0, \qquad (55)$$

$$=\; \frac{1}{2\pi}\int_{\lambda=0}^{\infty}\frac{1}{(u+\lambda)}\,e^{-uz'}e^{\lambda z}\lambda\,J_0(\lambda\rho)\,d\lambda, \qquad z<0, \qquad\qquad (56)$$

$$g_z^x(\mathbf{r};\mathbf{r}') \;=\; -\frac{1}{2\pi}\frac{(x-x')}{\rho}\int_{\lambda=0}^{\infty}\frac{1}{\lambda(u+\lambda)}e^{-u(z+z')}\lambda^2\,J_1(\lambda\rho)\,d\lambda, \qquad z\geq 0, \qquad (57)$$

$$=\; -\frac{1}{2\pi}\frac{(x-x')}{\rho}\int_{\lambda=0}^{\infty}\frac{1}{\lambda(u+\lambda)}e^{-uz'}e^{\lambda z}\lambda^2\,J_1(\lambda\rho)\,d\lambda, \qquad z<0, \qquad (58)$$

$$g_z^z(\mathbf{r};\mathbf{r}') \;=\; g^w(\mathbf{r};\mathbf{r}') \;-\; \frac{1}{2\pi}\int_{\lambda=0}^{\infty}\frac{1}{2u}\,e^{-u(z+z')}\,\lambda\,J_0(\lambda\rho)\,d\lambda, \qquad z\geq 0, \qquad (59)$$

$$=\; 0 \qquad\qquad z<0, \qquad\qquad\qquad\qquad\qquad\qquad\qquad\qquad\qquad\qquad (60)$$

where $u=\sqrt{\lambda^2-k_b^2}$, $\rho=\sqrt{(x-x')^2+(y-y')^2}$, and J_0 & J_1 are the Bessel functions of the first kind of orders 0 and 1. The above Hankel transforms are computed using the digital filtering routine of Anderson (1982).

Given the halfspace Green's functions, and the total electric field within the anomalous region, the electric field is calculated wherever required in the halfspace using eq. (44), and the magnetic field is calculated using eq. (26). The integrals are computed using Gaussian quadrature and the forms given in eqs. (38) & (42).

8. Examples

Here we present two examples: one a comparison with results from a DC resistivity modelling program since the form of our integral equation solution was strongly influenced by those for the DC problem, and one for an airborne electromagnetic transmitter-receiver geometry over a conductivity contrast of $100:10^{-4}$.

The model for the first example comprises a vertical prism of $0.2\,\mathrm{S/m}$ in a halfspace of $0.02\,\mathrm{S/m}$, as shown in Figure 2. The centre of the prism is $1000\,\mathrm{m}$ from the furthest end of the $100\,\mathrm{m}$ long grounded electric line source. The top surface of the prism is $100\,\mathrm{m}$ below the surface of the halfspace, and its extents in the x-, y- and z-directions are 120, 200 and $400\,\mathrm{m}$, respectively. The total electric field along a profile over the centre of the prism was computed, and the values are shown by the crosses in the top panel of Figure 3. A frequency of $3\,\mathrm{Hz}$ was used. The prism was divided into $5\times5\times5$ cells. The volume

integrations were carried out using $2 \times 2 \times 2$ nodes, and the surface integrals using 5×5 nodes. The electric field without the prism present, that is, the background field, is also shown in Figure 3. The real part of the secondary field is displayed in the bottom panel in Figure 3. The electric field for this model was also computed using the DC resistivity modelling program "DCIP3D" (Li, Oldenburg & Shekhtman, 1999), and is indicated by the squares in Figure 3. The real part of the electric field within the prism as computed using the integral equation solution is shown in Figure 4. The left panel in this figure shows the horizontal component of the total field over the uppermost layer of quadrature nodes, and the panel on the right shows the component in the x-z-plane for the cells down through the centre of the prism.

The second example is for a conductive cube in a resistive halfspace, as shown in Figure 5. The conductivity of the cube was 100 S/m, and that of the halfspace was 10^{-4} S/m. The vertical component of the magnetic field was computed 5 m from a unit vertical magnetic dipole source for a range of locations of the source-receiver pair over the cube (see Figure 5). The frequency was 900 Hz. The computed values of the secondary magnetic field are shown by the circles in Figure 6. The cube was divided into $5 \times 5 \times 5$ cells, the volume integrations were carried out using $3 \times 3 \times 3$ nodes, and the surface integrals using 15×15 nodes. The computed total electric field at the upper-most plane of volume integration nodes for the source at $x = 2.5$ m, $y = 0$ m is shown in Figure 7. The field for a sphere of the same conductivity and volume as the cube but in free space (Ellis, 1995) is indicated by the lines in Figure 6. It is clear from this figure that the integral equation solution presented here is successful even for such a large conductivity contrast as the one in this example.

9. Computational efficiency

The current implementation of our integral equation solution is slow. This is because of the large number of times the Green's functions and basis vectors are evaluated in the Gaussian quadrature integrations. The situation is exacerbated by the second level of integrations for the inner products required in the Galerkin approach. As an illustration, the second example in the preceding section (for the discretization of $5 \times 5 \times 5$ cells) took 3.5 hours on a 733 MHz Pentium III computer using $2 \times 2 \times 2$ nodes for the volume integrations and 5×5 nodes for the surface integrals, and took $4^{1}/_{4}$ days using $3 \times 3 \times 3$ nodes

for the volume integrations and 15×15 nodes for the surface integrals. (The results for these two cases were similar, but with noticeable improvement on the flanks of the responses shown in Figure 6 for the greater number of quadrature nodes.) For both these times, over 99 % was taken up with the integrations needed to construct the matrix equation. The introduction of efficient ways to compute the essentially convolution-type integrals is therefore needed to make the technique viable for general usage. However, even the current formulation is valuable in that it can supply an independent check on results obtained from other numerical solutions of the geophysical electromagnetic forward-modelling problem.

10. Conclusions

We have implemented edge element basis functions in the numerical solution of the electric field integral equation. We have also ensured that the form of the integral equation upon which our solution is based, especially once the discretization of the model has been introduced, reduces at zero frequency to that for the DC resistivity problem. We feel that the resulting treatment of charges, and hence current density, on the interfaces between cells of different conductivities, and between cells and the background, plays just as important a role as the use of the divergence free but not curl free edge element basis vectors. Tests to date have agreed well with published results and those from other algorithms, including those for models with large conductivity contrasts.

References

Anderson, W.L., 1982. Fast Hankel transforms using related and lagged convolutions, ACM Transactions on Mathematical Software, 8, 344–368.

Ellis, R.G., 1995. Airborne EM forward modeling in 3D, in 1994 Annual Report of the JACI Consortium, University of British Columbia.

Hohmann, G.W., 1975. Three-dimensional induced-polarization and electromagnetic modeling, Geophysics, 40, 309–324.

Hohmann, G.W., 1987. Numerical modeling for electromagnetic methods of geophysics: in Electromagnetic Methods in Applied Geophysics, M.N. Nabighian (ed.), SEG, Tulsa, OK.

Jin, J., 1993. The Finite Element Method in Electromagnetics, John Wiley, New York.

Li, Y. & D.W. Oldenburg, 1991. Aspects of charge accumulation in d.c. resistivity experiments, Geophysical Prospecting, 39, 803–826.

Li, Y., D.W. Oldenburg & Shekhtman, 1999. DCIP3D: A Program Library for Forward Modelling and Inversion of DC Resistivity and Induced Polarization Data over 3D Structures, in Report of the INDI Consortium, University of British Columbia.

Newman, G.A. & G.W. Hohmann, 1988. Transient electromagnetic responses of high-contrast prisms in a layered earth, Geophysics, 53, 691–706.

Slob, E.C. & P.M. van den Berg, 1999. Integral-equation method for modeling transient diffusive electromagnetic scattering: in Three-Dimensional Electromagnetics, M. Oristaglio & B. Spies (eds.), SEG, Tulsa, OK.

Snyder, D.D., 1976. A method for modeling the resistivity and IP response of two-dimensional bodies, Geophysics, 41, 997–1015.

Tai, C.-T., 1993. Dyadic Green Functions in Electromagnetic Theory, IEEE Press, New York, NY.

Ward, S.H. & G.W. Hohmann, 1987. Electromagnetic theory for geophysical applications: in Electromagnetic Methods in Applied Geophysics, M.N. Nabighian (ed.), SEG, Tulsa, OK.
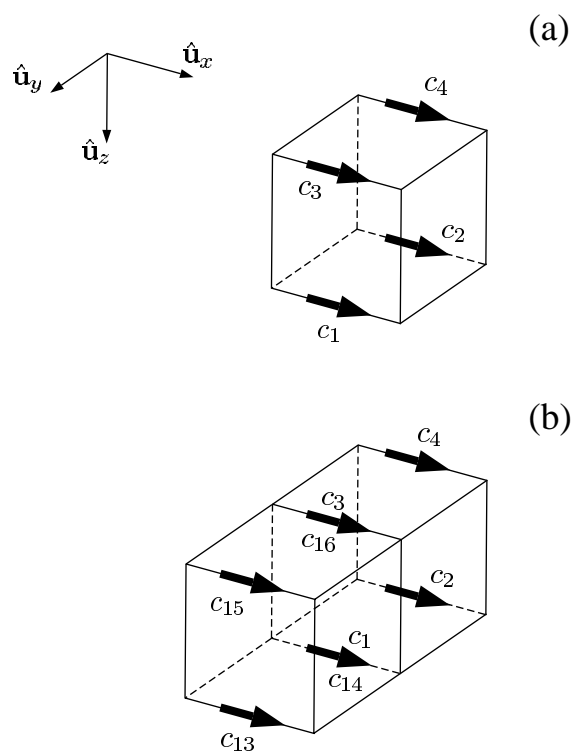
Figure 1.   (a) An example cell. $c_1 \ldots c_4$ are the coefficients of the four basis vectors that approximate the x-component of the total electric field within this cell. (b) The example cell and its neighbour in the positive y direction. $c_{13} \ldots c_{16}$ are the coefficients of the corresponding basis vectors in this neighbouring cell.

0   100   **1000**

100

X

500

Z
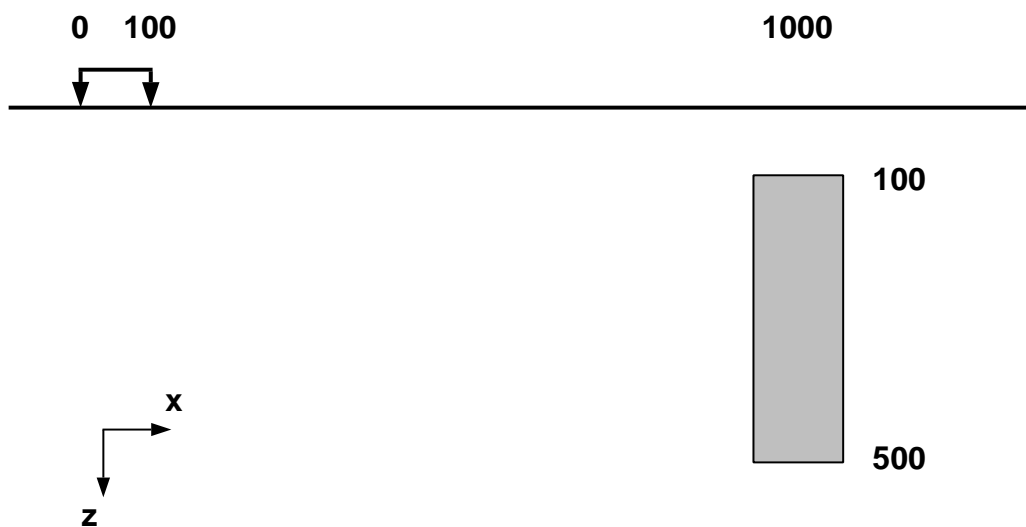
Figure 2.   The geometry of the first example presented in this paper. The halfspace background has a conductivity of 0.02 S/m. The prism has a conductivity of 0.2 S/m, and has extents of 120 and 200 m in the x- and y-directions, respectively, and is centred below the x-axis.

Lines − halfspace; crosses − with prism
Solid − real; dashed − imaginary

Crosses − integral equation
Squares − DC resistivity code
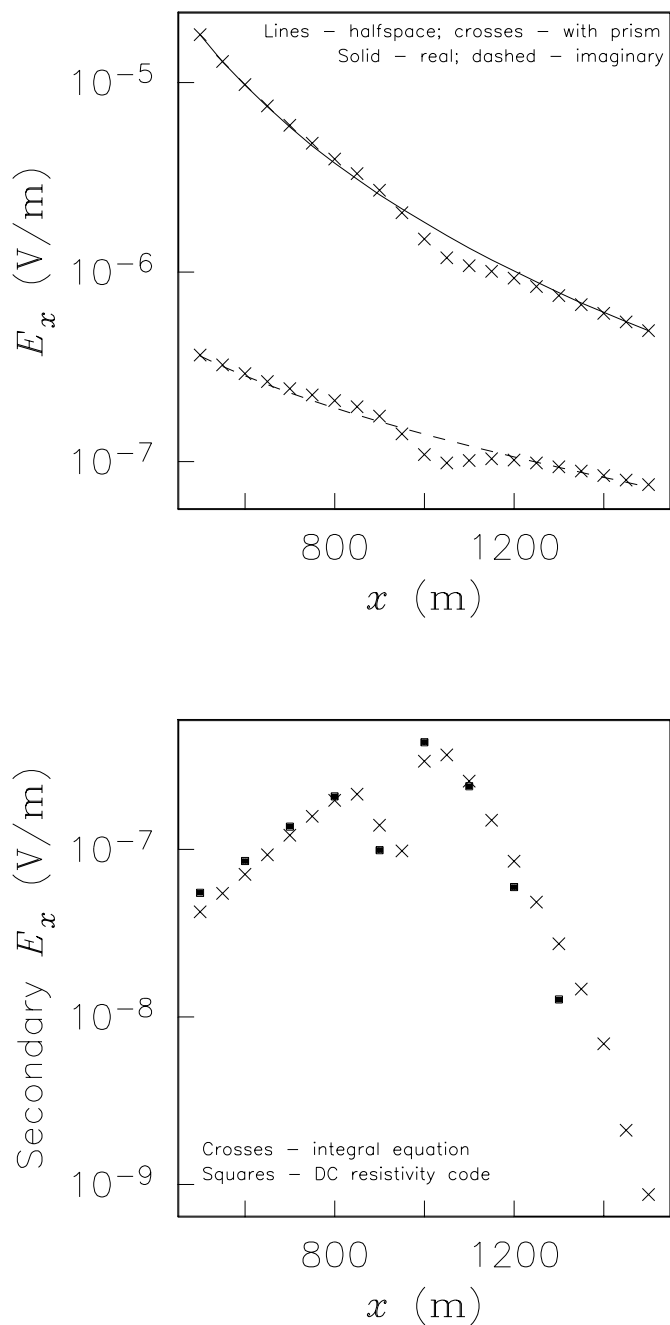
Figure 3. Top panel: the x-component of the background (lines) and total (crosses) electric fields on the surface of the halfspace over the top of the prism (which is centred at $x = 1000\,\text{m}$). Bottom panel: the real part of the secondary field as computed by the integral equation code presented in this paper (crosses), and the secondary field computed using the DC resistivity forward modelling code DCIP3D (squares).
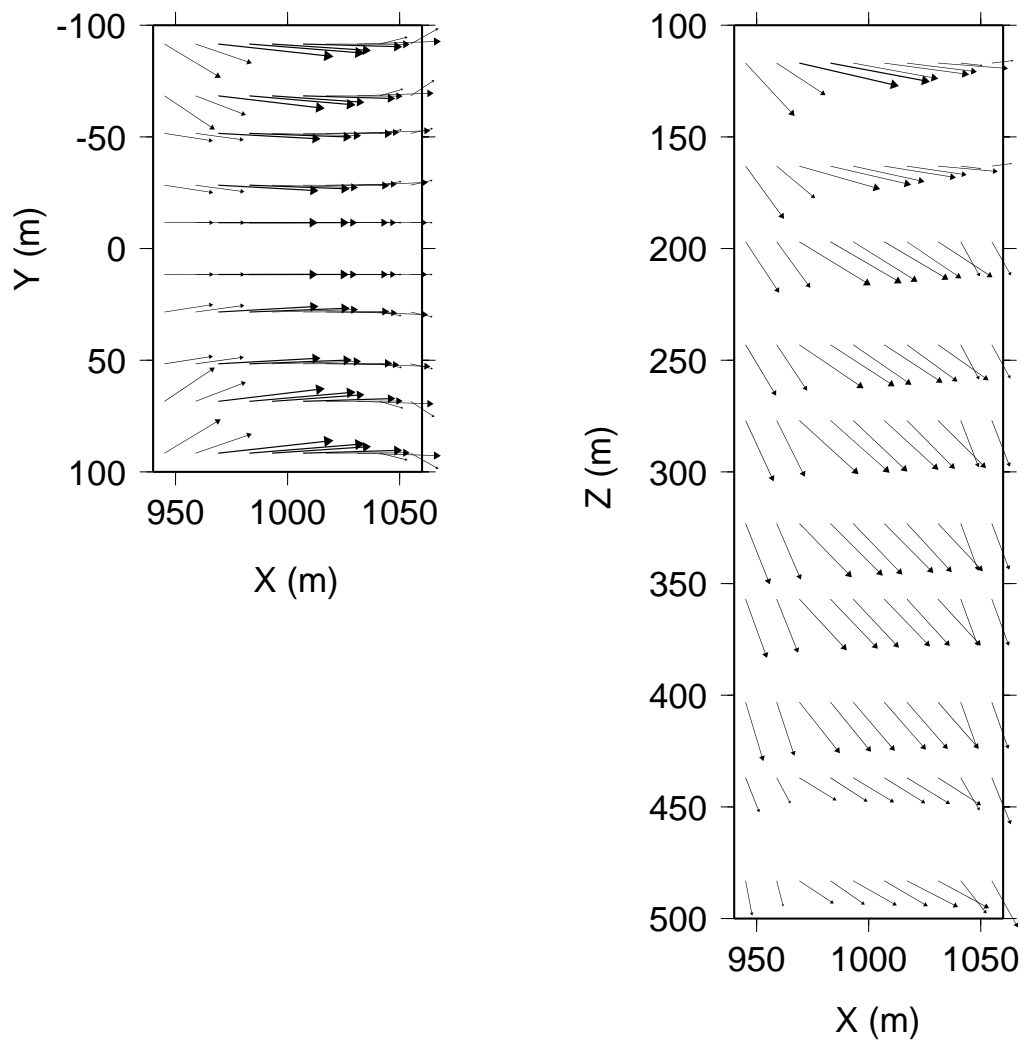
Figure 4. The real part of the computed total electric field within the prism. The prism was divided into $5 \times 5 \times 5$ cells with $2 \times 2 \times 2$ quadrature nodes within each cell. The left panel shows the field over the top-most plane of quadrature nodes, and the right panel shows the field in the cells down through the centre of the prism. The longest arrow corresponds to a field strength of 8.4×10^{-7} V/m.

Plan view   Side view

5

5

18

18

x

76

18

x

18

y

18
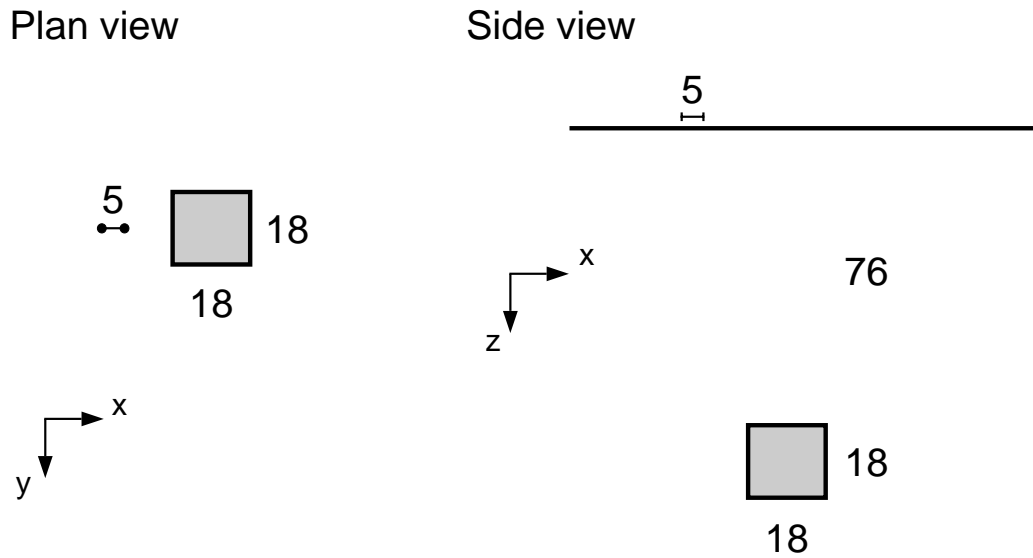
Figure 5. The geometry of the second example. A magnetic dipole source-receiver pair is considered. The cube has a conductivity of $100\,\mathrm{S/m}$, and the halfspace a conductivity of $10^{-4}\,\mathrm{S/m}$. The origin is on the Earth-air interface directly above the centre of the cube. All dimensions are in metres.
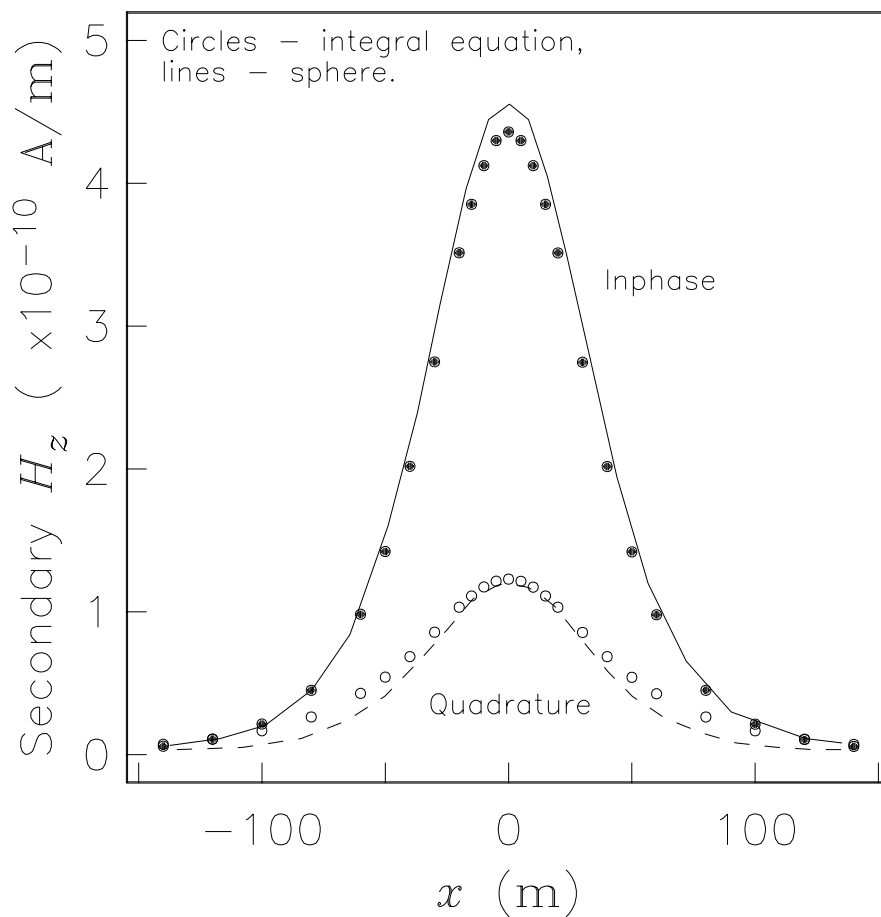
Figure 6.   The vertical component of the secondary magnetic field for the second example. The circles show the values computed using our integral equation solution. The lines are for an equivalent sphere in free space. The abscissa is the location of the centre of the source-receiver pair.
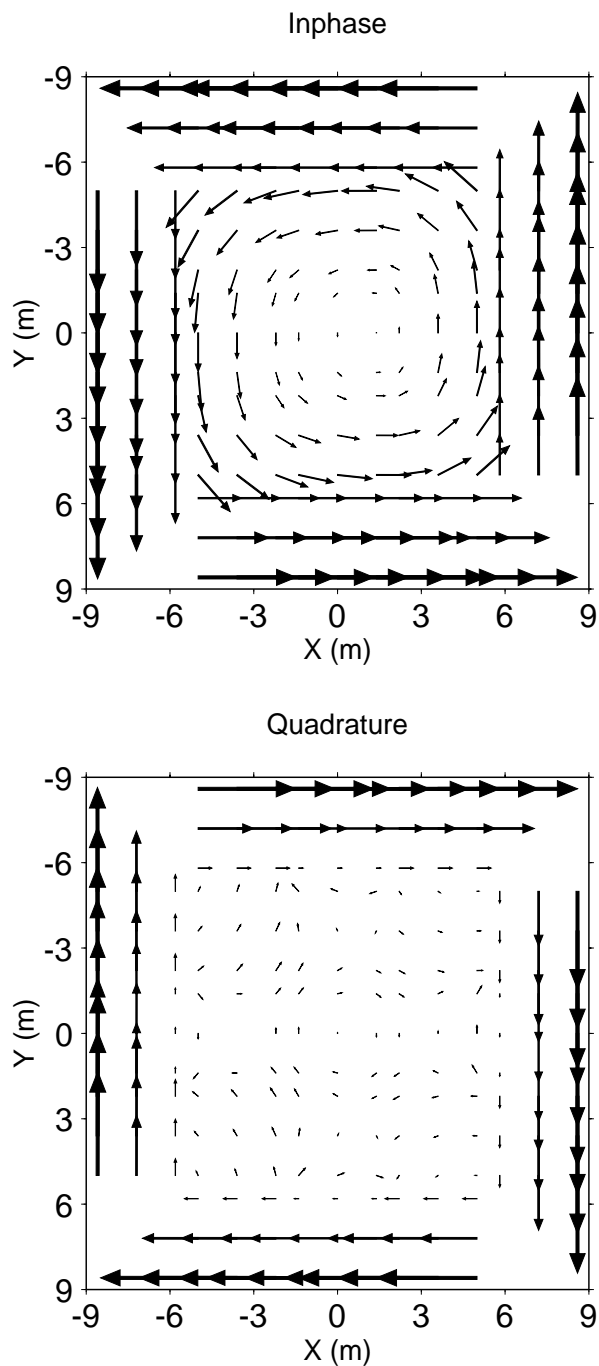
Figure 7.   The computed total electric field over the top plane of quadrature nodes for the source at $x = 2.5\,\mathrm{m}$, $y = 0\,\mathrm{m}$. The cube was divided into 5×5×5 cells, with 3×3×3 quadrature nodes within each cell. The longest arrow corresponds to a field strength of $4 \times 10^{-9}\,\mathrm{V/m}$.